Vol. 16(1), pp. 16-28, January-March, 2021
DOI: 10.5897/IJPS2020.4920
Article Number: 41DFF6B65991
ISSN 1992-1950

http://www.academicjournals.org/IJPS

International Journal of Physical Sciences

Full Length Research Paper

Stability and elastic anisotropy of diamond related $C_{8-y}B_y$ materials

G. Samukonga[1,2], A. Habanyama[1]* and N. K. Mumba[1]

[1]Department of Physics, Copperbelt University, P. O. Box 21692, Jambo Drive, Riverside, Kitwe 10101, Zambia.
[2]Department of Physics, Mukuba University, P. O. Box 20382, Itimpi, Garnerton, Kitwe 10101, Zambia.

Received 3 October 2020, Accepted 11 January, 2021

A number of potentially super-hard materials were examined using ab-initio methods. Low Gibbs free energy polymorphs of diamond-like materials for y = 0 to 7 in the stoichiometric type C_{8-y} B_y, were identified at absolute zero of temperature. These were proposed as possible super-hard materials with useful applications. The materials with y = 0 to 3, that is, diamond (C), cubic C_7B (c-C_7B), rhombohedral C_3B (r-C_3B) and orthorhombic C_5B_3 (o-C_5B_3) were found to be dynamically and mechanically stable. A diamond standard was used as a stable comparison. Results of their bulk modulus calculations suggest that these materials were potentially super-hard in character. Systematic trends were established, the hardness was observed to reduce with increasing boron content. The materials under study were all determined as being brittle with diamond being the most brittle, C_3B and C_5B_3 are the least brittle with *B/G* values of 1.32. Of the materials studied, diamond was determined to have the lowest degree of elastic anisotropy with a Universal Elastic Anisotropy Index of only 0.041 while C_5B_3 had the highest anisotropy of 1.160, making it the most susceptible to micro-cracks. Our electronic band structure studies of c-C_7B, which was predicted to be the hardest in the C_{8-y} B_y system after diamond, showed that the top of the valence band was about 1.7 eV above the Fermi level with a band gap between the valence and conduction bands, making c-C_7B a hole-type conductor having a likely increase in conductivity with increased applied hydrostatic pressure.

Key words: Phase stability, elastic anisotropy, ultra-hard material.

INTRODUCTION

Super-hard materials have important applications in high speed machining tools for cutting and drilling as well as abrasives and wear-resistant coatings because of their strength. Diamond is extremely hard but at high temperatures and in the presence of oxygen it becomes unstable due to oxidation reactions (John et al., 2002). It is not suitable for machining steel and other alloys of iron because of its redox reactions with iron and some other metallic elements (Nassau and Nassau, 1979) at temperatures exceeding 80 K. Cubic boron nitride (c-BN) is a super abrasive which is more thermally stable than diamond and is better suited for machining steel. However, despite the high oxidation resistance temperature and high chemical inertness of c-BN, it is only about half as hard as diamond (Singh, 1986). The possible replacement of both diamond and c-BN by better

*Corresponding author. E-mail: adrian.habanyama@cbu.ac.zm. Tel: +260 963313923.

performing super abrasives has motivated a lot of researcher interest.

An important frontier in high-pressure science and technology research has been the synthesis of novel ultra- or super-hard materials. Diamond anvil cells (DAC) are reported (Stavrou et al., 2016) to have been successfully used in synthesizing such materials under high pressure and temperature conditions.

Covalent bonds are strong and highly resistant to plastic and elastic deformations (Zhao et al., 2016). The predominant atomic binding mechanism in super-hard materials is therefore covalent bonding. The constituent atomic elements in these materials are often light, like C, B, O, and N (Habanyama et al., 2018) which are chemically suited for covalent bonding (Hu et al., 2016). Since covalent bonds are generally directional and short, the light elements are able to form highly shear resistant 3-dimentional networks.

A method of reducing diamond's susceptibility to oxidation and reaction with ferrous alloys is to dope it with boron. However, the highest possible doping concentration of boron in boron-doped diamond (BDD) is very low. The synthesis of new diamond-like compounds of carbon and boron is being considered as an effective method of achieving a much higher boron content. There have been recent developments in computational discovery of super-hard materials (Kvashnin et al., 2019) and ab-initio calculations of elastic constants (Mazhnik and Oganov, 2019; Niu et al., 2019). Recent theoretical work has also been carried out on diamond-like boron carbon nitrides (d-BC_xN) (He et al., 2019; Gao et al., 2018).

The Vickers hardness (H_V) of ultra-hard materials is known to be more than 40 GPa (Solozhenko and Gregoryanz, 2005). Materials with super-hard characteristics are known to have a value of the bulk modulus that exceeds 250 GPa (Lowther, 2000). Both the bulk and shear moduli have been used as scales to estimate the level of hardness of materials (Clerc, 1999).

A single crystal seldom exhibits a totally isotropic elastic response, essentially all known crystals exhibit some form of elastic anisotropy, meaning that the elastic moduli are generally dependent on the different crystal orientations. The degree of anisotropy in the properties of materials is very important in their application. The generation of micro-cracks and lattice distortions in materials is often related to the elastic anisotropy. Ledbetter and Migliori (2006) point out the effects of elastic anisotropy in dislocation dynamics, phase transformations and other crystal phenomena.

Energetic or thermodynamical stability is determined by the relative value of the system's Gibbs free energy,

$$G = E + PV - TS \,. \quad (1)$$

The internal energy is E, volume is V, pressure is P, temperature is T and the system's entropy is S. The most stable compound phase maximizes the chemical bond strength and has the lowest value of G. Our calculations involve ground state structures of compounds determined under a thermal limit conditions (that is, neglecting zero point motion) at zero-temperature (T = 0 K). In this case, the minimum Gibbs free energy is equivalent to the minimum enthalphy, H where,

$$H = E + PV \,. \quad (2)$$

In this work, we study the energetic, dynamical, mechanical and anisotropic properties of diamond-like materials for y = 0 to 7 in the stoichiometric type $C_{8-y}B_y$.

COMPUTATIONAL METHODS

The method of calculation applied in this work is based on the density functional theory (DFT) (Kohn and Sham, 1965). The Quantum Espresso (Giannozzi et al., 2009) software package implementation of DFT was adopted. The exchange-correlation interaction between the electrons was modeled using the Generalized Gradient Approximation as parameterized by Perdew, Burke and Ernzerhof (GGA-PBE) (Perdew et al., 1996). The ultra-soft pseudo-potential method was used to calculate the interaction between the electrons and the ion cores. The cut-off energy used for the plane-wave functions was 50 Ry, sampling of the k-point mesh in the Brillouin zone was 6×6×6 Monkhorst Pack (Monkhorst and Pack, 1976). The convergence threshold of the self-consistent field (SCF) was within 10^{-3} eV/atom.

The initial structure consisted of eight atoms in a unit with boron or carbon atoms placed at diamond lattice positions in a ratio that represented a particular stoichiometric value of y. The lattice positions and atomic types at each position were stored in matrix arrays. A C++ template library for linear algebra called Eigen (http://eigen.tuxfamily.org/) was used to randomise the atomic placement. Variable-cell dynamics calculations were performed on the starting cell to optimize the atomic position geometry and cell parameters using the Quantum Espresso (Giannozzi et al., 2009) package. This was achieved by performing some relaxation operations which allowed the positions of the atoms to adjust in accordance with the relative forces between them while allowing the unit cell to vary; equilibrium atomic structures were thereby achieved. The space-group and symmetry operations of these equilibrium configurations were identified using the utility program, SGROUP (Yanchitsky and Timoshevskii, 2001).

The procedure of randomising the atomic placement (using Eigen) in the starting cell, variable-cell relaxation (using Quantum Espresso) and identification of the final converged configurations (using SGROUP), was carried out several times for each value of y in $C_{8-y}B_y$ where y = 0 to 7. The crystal structures that resulted from the same value of y had similar stoichiometry and were polymorphs. Calculations were carried out on these structure to determine the configurations with the lowest value of the Gibbs free energy, G for each value of y in $C_{8-y}B_y$ where y = 0 to 7, at absolute zero of temperature. These eight configurations were then subjected to dynamical stability tests.

A material's vibrational spectrum needs to be analyzed in order to establish its dynamical or vibrational stability. The criterion for this aspect of stability is the nonappearance of imaginary phonons, that is, frequencies of vibration that are not positive in the dispersion calculations on phonons or lattice vibrations at reciprocal lattice vectors in the Brillouin zone. Phonon dispersion frequencies were obtained for specific modes of vibration using the Quantum Espresso implementation of the density functional perturbation or

"linear response" theory (Baroni et al., 1987; Giannozzi et al., 1991).

The structures which were found to be dynamically stable were constructed and visualized by the Xcrysden software package (Kokalj, 2003) after which they were tested for mechanical or elastic stability which considers the second order elastic constants of a material. Elastic stiffness and compliance constants were calculated using the elastic package (Golesorkhtabar et al., 2013).

Three types of averaging calculations were carried out to determine the shear and bulk moduli of the various compounds: the Voigt (1928) calculation where the strain is taken to be uniform, Reuss and Angew (1929) calculation where the stress is taken to be uniform and Hill (1963) values which are the averages of the combined Reuss and Voigt values.

For Voigt bulk, B_V and shear, G_V moduli values are calculated as:

$$B_V = (1/9)[(C_{33} + C_{22} + C_{11}) + 2(C_{23} + C_{13} + C_{12})] \quad (3)$$

and

$$G_V = (1/15)[(C_{33} + C_{22} + C_{11}) - (C_{23} + C_{13} + C_{12}) + 3(C_{66} + C_{55} + C_{44})] \quad (4)$$

respectively, where C_{ij} are the stiffness constants.

For Voigt bulk, B_R and shear, G_R moduli values are calculated as:

$$B_R = 1/[(S_{33} + S_{22} + S_{11}) + 2(S_{23} + S_{13} + S_{12})] \quad (5)$$

and

$$G_R = 15/[4(S_{33} + S_{22} + S_{11}) - (S_{23} + S_{13} + S_{12}) - 3(S_{66} + S_{55} + S_{44})] \quad (6)$$

respectively, where S_{ij} are the compliances.

The bulk and shear values are averaged to give the Hill values as:

$$G_H = \frac{1}{2}(G_V + G_R) \quad (7)$$

and

$$B_H = \frac{1}{2}(B_V + B_R). \quad (8)$$

The respective Hill values of the Young modulus, E_H and Poisson ratio, ν_H are obtained from the expressions:

$$E_H = \frac{9B_H G_H}{3B_H + G_H} \quad (9)$$

and

$$\upsilon_H = \frac{3B_H - 2G_H}{2(3B_H + G_H)}. \quad (10)$$

The elastic constant results presented for all materials in this work are Hill-averaged, unless indicated otherwise.

The bulk modulus for crystals that exhibit cubic symmetry is the same in all directions. Cubic elastic anisotropy is therefore determined by the shear anisotropy alone. There are both bulk and shear anisotropic contributions in crystals that are not cubic. An appropriate way to quantify the combined bulk and shear degree of anisotropy is by using the universal elastic anisotropy index, A_U (Ranganathan and Ostoja-Starzewski, 2008) which is given by,

$$A_U = 5\frac{G_V}{G_R} + \frac{B_V}{B_R} - 6. \quad (11)$$

If a single crystal is isotropic in both bulk and shear then, $B_V = B_R$ and $G_V = G_R$, making A_U equal to zero. In cubic crystals $B_V = B_R$ but $G_V \neq G_R$. The degree of anisotropy is determined by the extent of the departure of A_U from zero.

RESULTS

The crystal structures that resulted from the same value of y had similar stoichiometry and were polymorphs. Calculations were carried out on these structure to determine the configurations with the lowest value of the Gibbs free energy, G for each value of y in $C_{8-y}B_y$ where y = 0 to 7, at absolute zero of temperature. The resulting eight configurations are listed in Table 1. The structures were then tested for dynamical stability. Our phonon calculation results at the Brillouin zone center (the Γ point) are also presented in Table 1. The value, y = 0 represents a diamond standard, used as a stable comparison.

The calculations of the results shown in Table 1 covered 24 frequencies for each material but the table only shows the lowest and highest 6 results, all other frequencies were positive. This table shows that the materials with y = 0 to 3, that is, diamond (C), C_7B, C_3B (or C_6B_2) and C_5B_3 have no negative phonon frequencies at the Γ point of the Brillouin zones, indicating possible dynamical stability. All the other structures showed some negative frequencies indicating dynamical instability. Further phonon calculations, to complete the test for dynamical stability, were therefore only carried out on C_7B, C_3B and C_5B_3. Further phonon calculations for diamond are not included here since the stability of diamond is well established.

Figure 1 shows some high symmetry lines and points in the first Brillouin zone of the orthorhombic lattice structure.

Phonon calculations were carried out at all the eight high symmetry points as shown in Figure 1, for the orthorhombic C_5B_3 structure, the results are presented in Table 2. The calculations in Table 2 covered 24 frequencies for each symmetry point, but as in Table 1, we only picked the lowest and highest 6 results, all other frequencies were positive. Each frequency is presented in units of both THz (the upper value) and cm^{-1} (the lower value). The k-space coordinates of the Brillouin zone indicated in Table 2 are in integral units of a reciprocal lattice multiplying factor of π divided by the corresponding lattice parameters. It is seen in Table 2 that there are no negative phonon frequencies at any of the eight high symmetry points of the Brillouin zone; this structure is therefore dynamically stable. In Table 2, acoustic mode vibrations correspond to the low frequencies while the higher frequencies indicate vibrations in the optical mode.

Table 1. Results of phonon calculations for low Gibbs free energy, $C_{8-y}B_y$ compounds.

Material and crystal structure	C Cubic ($Fd\bar{3}m$)	C_7B Cubic ($P\bar{4}3m$)	C_3B (Rhombohedral (R3m)	C_5B_3 Orthorhombic (Pnma)	CB Orthorhombic (Pnma)	C_3B_5 Orthorhombic (Pnma)	CB_3 Rhombohedral (R3m)	CB_7 Cubic ($P_{\bar{4}}3m$)
Frequency number	cm^{-1}	cm^{-1}	cm^{-1}	cm^{-1}	cm^{-1}	cm^{-1}	cm^{-1}	cm^{-1}
1	186	148	26	46	-1675	-181	-297	-182
2	186	148	48	52	-171	-80	-297	-182
3	806	148	48	87	-138	-48	-113	-182
4	806	671	505	361	-63	98	-61	87
5	806	671	590	429	73	310	-61	87
6	806	671	590	450	80	380	195	87
19	1207	1054	1066	989	800	871	951	649
20	1207	1054	1066	1000	813	955	951	649
21	1207	1093	1084	1067	1032	985	1006	927
22	1303	1093	1096	1077	1120	995	1061	1014
23	1303	1093	1102	1081	1154	1110	1061	1014
24	1303	1115	1102	1083	1221	1139	1156	1014

y = 0 to 7, at the Γ point of the Brillouin zones. Only 12 out of 24 frequencies studies for each material are shown in the table, all other frequencies were positive.

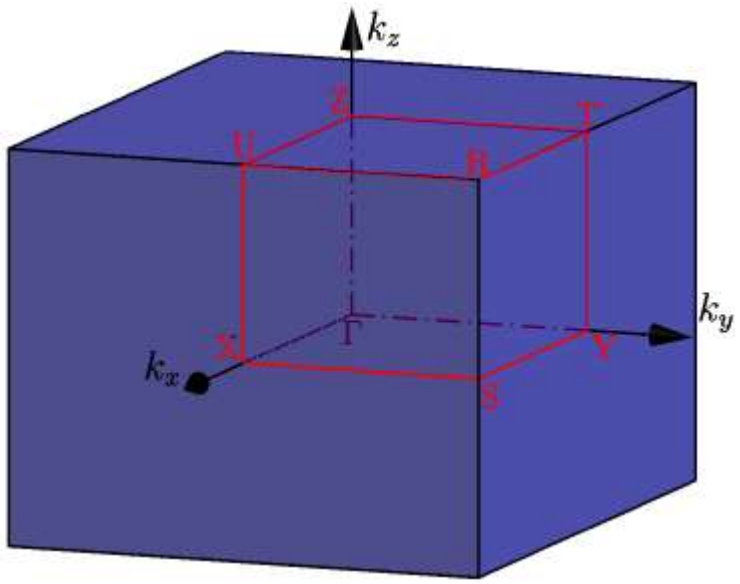

Figure. 1. First Brillouin zone of the orthorhombic lattice showing some high symmetry lines and points.

If all sides of the first Brillouin zone of the orthorhombic lattice were drawn with equal lengths then Figure 1 would represent the Brillouin zone of a cubic lattice. Phonon calculations were carried out at all the eight high symmetry points as shown in Figure 1, for the cubic C_7B structure, the results are presented in Table 3. The results in Table 3 show the lowest and highest 6 frequencies, with all other frequencies being positive, as explained in the case of C_5B_3.

It is seen in Table 3 that there are no negative phonon frequencies at any of the eight high symmetry points of the Brillouin zone; this structure is therefore also dynamically stable.

Phonon calculations for C_3B were carried out at eight k-

Table 2. Results of phonon calculations for the orthorhombic C_5B_3 structure at Γ, Z, T, Y, S, X, U and R high symmetry points of the Brillouin zone.

Γ - point k-space coordinates: (0.0,0.0,0.0) Frequency: (TH z/cm^{-1})	Z - point k-space coordinates: (0.0,0.0,1.0) Frequency: (TH z/cm^{-1})	T - point k-space coordinates: (0.0,1.0,1.0) Frequency: (TH z/cm^{-1})	Y - point k-space coordinates: (0.0,1.0,0.0) Frequency: (TH z/cm^{-1})	S - point k-space coordinates: (1.0,1.0,0.0) Frequency: (TH z/cm^{-1})	X - point k-space coordinates: (1.0,0.0,0.0) Frequency: (TH z/cm^{-1})	U - point k-space coordinates: (1.0,0.0,1.0) Frequency: (TH z/cm^{-1})	R - point k-space coordinates: (1.0,1.0,1.0) Frequency: (TH z/cm^{-1})
1.387391	2.105485	4.168883	4.015138	4.168997	2.106805	2.599211	4.579857
46.27836	70.23140	139.0589	133.9305	139.0627	70.27546	86.70033	152.7675
1.567703	2.997539	4.723377	4.028546	4.723421	2.997709	3.421805	5.236349
52.29293	99.98714	157.5549	134.3778	157.5563	99.99282	114.1391	174.6657
2.616957	3.007458	5.875216	5.586029	5.874522	3.007610	3.971454	5.947808
87.29229	100.3179	195.9761	186.3298	195.9529	100.3230	132.4734	198.3975
10.810605	11.435570	11.599394	10.867298	11.599428	11.435565	11.979791	12.304007
360.60295	381.44954	386.91413	362.49403	386.91528	381.44940	399.60280	410.41749
12.850011	12.391740	12.617579	13.150957	12.617377	12.391738	13.375969	13.359577
428.63021	413.34394	420.87714	438.66871	420.87038	413.34389	446.17431	445.62751
13.488162	14.429497	14.535573	13.479501	14.535595	14.429499	15.117790	15.251466
449.91665	481.31620	484.85451	449.62775	484.85526	481.31626	504.27519	508.73416
29.646463	29.750770	29.679222	29.574427	29.679126	29.750771	29.829252	29.766395
988.89957	992.37887	989.99229	986.49669	989.98906	992.37889	994.99674	992.90005
29.971169	30.092797	29.985140	29.860217	29.985186	30.092779	30.053687	29.979707
999.73059	1003.7876	1000.1966	996.02961	1000.1981	1003.7870	1002.4830	1000.0153
31.986568	31.912550	31.818506	31.869566	31.818578	31.912623	31.781355	31.693800
1066.9570	1064.4880	1061.3511	1063.0543	1061.3535	1064.4905	1060.1118	1057.1913
32.277680	32.368624	32.198484	32.040780	32.198575	32.368623	32.405758	32.257897
1076.6674	1079.7010	1074.0258	1068.7653	1074.0288	1079.7010	1080.9397	1076.0076
32.412637	32.414004	32.307504	32.245813	32.307195	32.413976	32.506030	32.387860
1081.1691	1081.2147	1077.6623	1075.6045	1077.6520	1081.2138	1084.2844	1080.3427
32.451446	32.486772	32.331805	32.296109	32.331709	32.486784	32.620144	32.467848
1082.4637	1083.6420	1078.4729	1077.2822	1078.4697	1083.6424	1088.0908	1083.0108

The **k**-space coordinates indicated in the table are in units of π divided by the corresponding lattice parameters.

point coordinates in the Brillouin zone of the rhombohedral structure of the trigonal system, in a similar way as was done for C_5B_3 and C_7B. The results are shown in Table 4. Table 4 shows that rhombohedral C_3B is dynamically stable. The details of the crystal systems for the materials that were found to be dynamically stable are shown in the following.

Firstly, the carbon-cubic diamond structure which has the Hermann Mauguin Space Group, $Fd\bar{3}m$ [SG number index, 227]. This structure has a face-centred cubic Bravais lattice with a Point Group, $m\bar{3}m$. The 'F' in the space group signifies that it is a face-centred lattice type. Diamond is already well studied and is only being used here as a standard to which the other materials will be compared.

Secondly, a C_7B structure with the Hermann Mauguin Space Group, $P\bar{4}3m$ [space group number index, 215], which has a primitive cubic Bravais lattice with the Point Group, $\bar{4}3m$. The 'P' in the space group signifies that it is a primitive lattice type. We will refer to this cubic material as *c*-C_7B, in short.

Thirdly, a C_3B (C_6B_2) structure with the Hermann Mauguin Space Group, R3m [space group number index, 160], which has a rhombohedral structure of the trigonal Bravais lattice crystal system with the Point Group, 3m. The 'R' in the space group signifies that it is a rhombohedral lattice type. We will refer to this rhombohedral material as being *r*-C_3B.

Fourthly, a C_5B_3 structure with the Hermann Mauguin Space Group, Imm2 [space group number index, 44], which has a body-centred orthorhombic Bravais lattice with the Point Group, mm2. The 'I' in the space group signifies that it is a body-centred lattice type. We will refer to this orthorhombic material as being *o*-C_5B_3.

Table 3. Results of phonon calculations for the cubic C_7B structure at Γ, Z, T, Y, S, X, U and R high symmetry points of the Brillouin zone.

Γ - point k-space coordinates: (0.0,0.0,0.0) Frequency: (TH z/cm^{-1})	Z - point k-space coordinates: (0.0,0.0,1.0) Frequency: (TH z/cm^{-1})	T - point k-space coordinates: (0.0,1.0,1.0) Frequency: (TH z/cm^{-1})	Y - point k-space coordinates: (0.0,1.0,0.0) Frequency: (TH z/cm^{-1})	S - point k-space coordinates: (1.0,1.0,0.0) Frequency: (TH z/cm^{-1})	X - point k-space coordinates: (1.0,0.0,0.0) Frequency: (TH z/cm^{-1})	U - point k-space coordinates: (1.0,0.0,1.0) Frequency: (TH z/cm^{-1})	R - point k-space coordinates: (1.0,1.0,1.0) Frequency: (TH z/cm^{-1})
4.427654	4.605549	4.605577	4.605549	4.605590	4.605549	4.605549	4.667695
147.6906	153.6245	153.6254	153.6245	153.6259	153.6245	153.6245	155.6975
4.427654	4.605549	4.607911	4.605549	4.608187	4.605549	4.607935	4.667695
147.6906	153.6245	153.7033	153.6245	153.7125	153.6245	153.7041	155.6975
4.427654	4.605549	4.831492	4.605549	4.831661	4.605549	4.831351	4.949015
147.6906	153.6245	161.1612	153.6245	161.1668	153.6245	161.1565	165.0813
20.12885	19.74729	20.75952	19.74731	20.75909	19.74731	20.75948	21.62326
671.4264	658.6988	692.4631	658.6993	692.4487	658.6995	692.4617	721.2743
20.12885	19.74731	20.95735	19.74731	20.95736	19.74731	20.95730	21.72804
671.4264	658.6993	699.0621	658.6993	699.0624	658.6995	699.0605	724.7696
20.12885	19.74731	21.31270	19.74731	21.31275	19.74731	21.31279	21.72804
671.4264	658.6993	710.9153	658.6993	710.9169	658.6995	710.9182	724.7696
31.60167	31.46595	31.58675	31.46594	31.58666	31.46595	31.58665	31.61542
1054.118	1049.591	1053.620	1049.591	1053.617	1049.591	1053.617	1054.577
31.60167	31.46595	31.60149	31.46595	31.60147	31.46595	31.60147	31.61542
1054.118	1049.591	1054.112	1049.591	1054.111	1049.591	1054.111	1054.577
32.76656	32.50473	32.78057	32.50466	32.78056	32.50473	32.78059	32.82877
1092.975	1084.241	1093.442	1084.238	1093.442	1084.241	1093.442	1095.050
32.76656	32.50473	32.80772	32.50466	32.80773	32.50473	32.80778	32.83906
1092.975	1084.241	1094.347	1084.238	1094.348	1084.241	1094.349	1095.393
32.76656	32.50473	32.80792	32.50466	32.80836	32.50473	32.80821	32.83906
1092.975	1084.241	1094.354	1084.238	1094.369	1084.241	1094.364	1095.393
33.42854	33.44330	33.44332	33.44330	33.44330	33.44330	33.44331	33.46691
1115.056	1115.548	1115.549	1115.548	1115.548	1115.548	1115.549	1116.336

The **k**-space coordinates indicated are in units of π divided by the corresponding lattice parameters.

Crystal diagrams of these four structures were constructed and visualized by the Xcrysden software package (Kokalj, 2003); they are as shown in Figure 2a and b followed by Figure 3a and b, respectively.

Previous theoretical studies (Sun et al., 2001; Nozaki and Itoh, 1996), on covalent bonding dominated compound structures of the ternary B-C-N system (which includes the binary B-C system), indicated that no B-B bonds were expected to exist in the crystal structures. This is because B-B bonds would effectively increase the total energy of the system hence making the structures less stable. It can be seen in Figures 2 and 3 that our diagrams are consistent with the results of these previous studies.

Elastic stiffness and compliance constants were calculated using the Elastic package (Golesorkhtabar et al., 2013) for the four materials that were identified as being dynamically stable; the results are shown in Table 5.

The materials in Table 5 were determined to be mechanically stable, as discussed subsequently. This qualified these materials for the determination of their bulk and other moduli, Hill values of these moduli are shown in Table 6. The table also shows the *B*/*G* ratio and the Poison ratio.

Table 7 presents the Voigt and Reuss bulk and shear moduli together with the universal elastic anisotropy index, calculated using Equation 11.

Table 7 shows that of the three predicted materials, that is, *c*-C_7B, *r*-C_3B and *o*-C_5B_3, it is C_7B that seems to be the most promising in terms of hardness. The electronic energy band structure of cubic C_7B was calculated in order to characterize some of its electronic properties.

Table 4. Results of phonon calculations for the rhombohedral C_3B structure at eight high symmetry points of the Brillouin zone.

Γ - point k-space coordinates: (0.0,0.0,0.0) Frequency: (TH z/cm^{-1})	k-space coordinates: (0.0,0.0,1.0) Frequency: (TH z/cm^{-1})	k-space coordinates: (0.0,1.0,1.0) Frequency: (TH z/cm^{-1})	k-space coordinates: (0.0,1.0,0.0) Frequency: (TH z/cm^{-1})	k-space coordinates: (1.0,1.0,0.0) Frequency: (TH z/cm^{-1})	k-space coordinates: (1.0,0.0,0.0) Frequency: (TH z/cm^{-1})	k-space coordinates: (1.0,0.0,1.0) Frequency: (TH z/cm^{-1})	k-space coordinates: (1.0,1.0,1.0) Frequency: (TH z/cm^{-1})
0.789661	1.559110	2.051128	1.558858	2.055059	1.558965	2.443306	2.497398
26.34026	52.00630	68.41825	51.99789	68.54939	52.00146	81.49990	83.30423
1.433620	2.144885	2.829444	2.139334	2.827949	2.139408	2.482183	3.126913
47.82041	71.54566	94.38008	71.36049	94.33022	71.36298	82.79669	104.3025
1.433620	2.802328	3.940311	2.804190	3.941992	2.802733	3.345743	4.436604
47.82041	93.47559	131.4346	93.53771	131.4906	93.48909	111.6019	147.9891
15.126597	15.923090	15.818824	15.923059	15.818791	15.923051	16.311675	16.666607
504.56896	531.13712	527.65917	531.13606	527.65806	531.13580	544.09891	555.93816
17.698805	17.818545	17.874093	17.818326	17.874096	17.818342	17.914171	17.954558
590.36858	594.36267	596.21558	594.35537	596.21567	594.35591	597.55243	598.89958
17.698805	17.968709	18.180780	17.968704	18.180814	17.968693	17.991200	18.298631
590.36858	599.37160	606.44555	599.37144	606.44668	599.37107	600.12182	610.37663
31.942236	32.109788	31.856979	32.109853	31.856831	32.109910	31.968891	31.911427
1065.4783	1071.0672	1062.6344	1071.0693	1062.6294	1071.0712	1066.3674	1064.4506
31.942236	32.166117	32.168713	32.166141	32.168789	32.166128	32.096968	32.197890
1065.4783	1072.9461	1073.0327	1072.9469	1073.0353	1072.9465	1070.6396	1074.0059
32.504106	32.532951	32.565338	32.532939	32.565386	32.532974	32.519228	32.540792
1084.2202	1085.1824	1086.2627	1085.1820	1086.2643	1085.1832	1084.7246	1085.4439
32.855045	33.012073	33.091105	33.012070	33.090855	33.012107	33.023181	33.128682
1095.9263	1101.1642	1103.8004	1101.1641	1103.7921	1101.1653	1101.5347	1105.0538
33.028584	33.092285	33.213691	33.091922	33.214608	33.092021	33.133005	33.270926
1101.7149	1103.8398	1107.8894	1103.8276	1107.9200	1103.8310	1105.1980	1109.7986
33.028584	33.155657	33.299551	33.155638	33.299597	33.155664	33.185767	33.366260
1101.7149	1105.9536	1110.7534	1105.9530	1110.7549	1105.9539	1106.9580	1112.9786

The **k**-space coordinates indicated are in units of π divided by the corresponding rhombohedral lattice parameters.

The **k**-point path used in this calculation, with reference to Figure 1, was: $\Gamma \to R \to Z \to T \to Y \to S \to \Gamma \to X$. Figure 4 shows the energy band diagram of *c*-C_7B under zero applied pressure where the origin of the energy axis is placed at the Fermi level, E_F.

The electronic band structure in Figure 4 shows that the highest valence energy band of the material crosses over the Fermi level up to about 1.7 eV above it. On the other hand, Figure 4 also shows a band gap between the top of the valence band and the bottom of the conduction band. This type of band structure configuration is indicative of hole-type conductivity. The material, *c*-C_7B is therefore a hole-type conductor.

The evolution of the Fermi energy, E_F at varying applied hydrostatic pressures from 0 to 2500 kbars was calculated relative to the Fermi energy at zero pressure, $E_F^{(0)}$ and plotted as a function of the applied pressure, as presented in Figure 5.

It is seen in Figure 5 that the relative Fermi energy increases monotonically with increased applied pressure. However, the curvature in the graph suggests that saturation would eventually be arrived at with further increase in applied pressure. An increase in Fermi energy with applied pressure has been associated with increased conductivity (Ghosh et al., 2016).

DISCUSSION

Materials with super-hard characteristics are known to have a value of the bulk modulus that exceeds 250 GPa (Lowther, 2000). Table 6 indicates that our materials with y = 0 to 3 could potentially have super-hard characteristics.

The original conditions for mechanical stability were

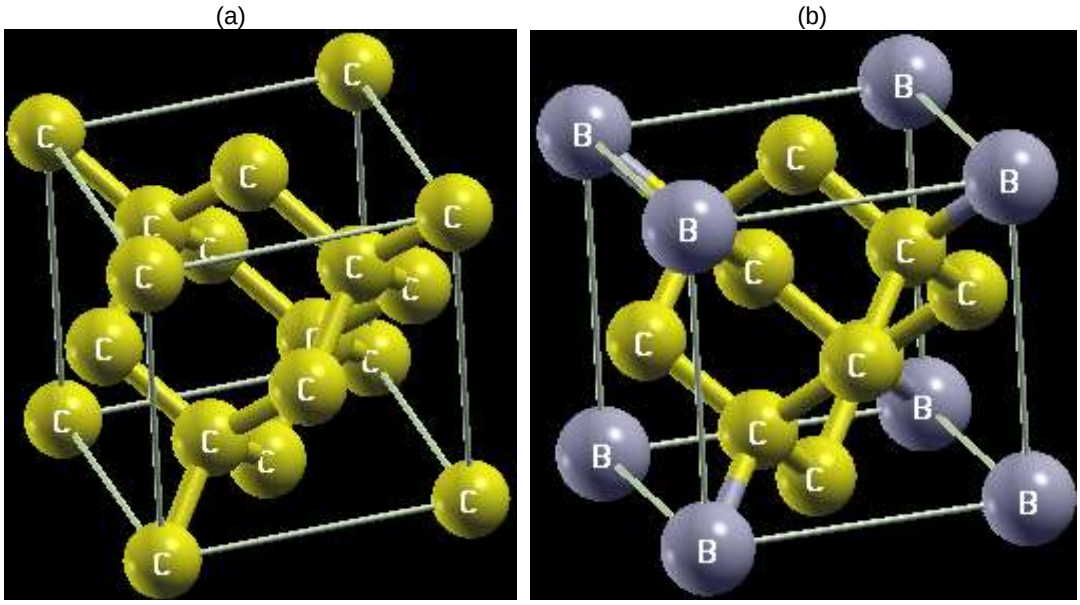

Figure 2. (a) The carbon-cubic diamond structure with Hermann Mauguin Space Group, $Fd\bar{3}m$ [SG number index, 227]. This was used as a standard for comparison. (b) The cubic C_7B structure with the Hermann Mauguin Space Group, $P\bar{4}3m$ [SG index, 215] and Point Group, $\bar{4}3m$.

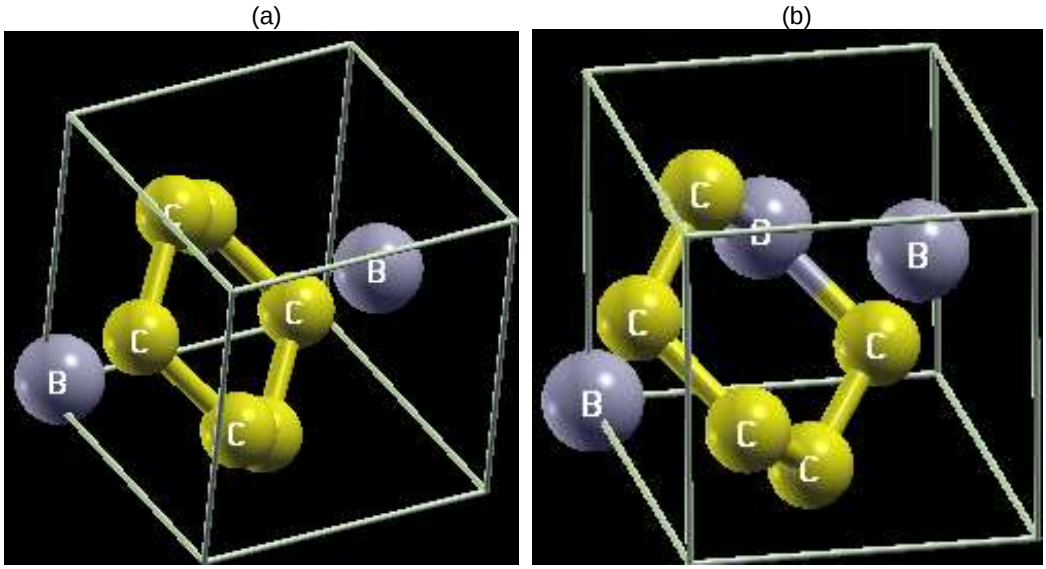

Figure 3. (a) The C_3B (C_6B_2) structure with the Space Group, R3m [space group number index, 160], which has a rhombohedral structure of the trigonal Bravais lattice crystal system with the Point Group, 3m. (b) The orthorhombic structure with the Hermann Mauguin Space Group, Imm2 [SG index, 44] and Point, Group, mm2.

proposed by Born-Huang (1954). In the current work, we adopt the modified conditions of Mouhat and Coudert (2014). A necessary although insufficient Born condition is that there should be no negative diagonal elements, that is, $C_{ii} > 0, \forall i$. It is seen in Table 5 that all the diagonal elements are positive for the compounds studied.

A second condition which is necessary but insufficient for Born stability is,

$$\left(C_{ij}\right)^2 < C_{ii}C_{jj}\forall i,j. \quad (12)$$

Table 5. Independent stiffness constants, C_{ij} and compliances, S_{ij} for $C_{8-y}B_y$ materials where y = 0 to 3.

Material	Crystal Structure	Stiffness matrix elements, C_{ij} (GPa) and compliances, S_{ij} ($\times 10^{-5}$ GPa^{-1})									
		C_{11}	C_{12}	C_{13}	C_{14}	C_{22}	C_{23}	C_{33}	C_{44}	C_{55}	C_{66}
		S_{11}	S_{12}	S_{13}	S_{14}	S_{22}	S_{23}	S_{33}	S_{44}	S_{55}	S_{66}
Diamond C	Cubic	1064	133	-	-	-	-	-	561	-	-
	($Fd\bar{3}m$)	97	-11	-	-	-	-	-	178	-	-
C_7B	Cubic	689	237	-	-	-	-	-	476	-	-
	($P\bar{4}3m$)	176	-45	-	-	-	-	-	210	-	-
C_3B	Rhombohedral	612	193	194	-72	-	-	612	358	-	-
	(R3m)	201	-55	-46	51	-	-	193	300	-	-
C_5B_3	Orthorhombic	455	264	98	-	604	285	547	334	303	334
	(Imm2)	296	-139	19	-	284	-123	243	300	330	300

Table 6. Hill bulk moduli, B, shear moduli, G and Young moduli, E for the four dynamically stable materials.

Material	Crystal Structure	Bulk Modulus (GPa)	Shear Modulus (GPa)	Young Modulus (GPa)	B/G	Poison Ratio, ν
Diamond C	Cubic F ($Fd\bar{3}m$)	443	521	1122	0.850	0.08
C_7B	Cubic ($P\bar{4}3m$)	388	353	812	1.099	0.15
C_3B	Rhombohedral	333	253	606	1.316	0.20
C_5B_3	Orthorhombic	309	235	563	1.315	0.20

The B/G ratio and Poison ratio are also presented.

Table 7. The Voigt and Reuss bulk and shear moduli together with the universal elastic anisotropy index for the materials.

Material	Crystal Structure	B_V (GPa)	B_R (GPa)	G_V (GPa)	G_R (GPa)	Universal Elastic Anisotropy Index, A_U	Percentage anisotropy (%)
Diamond C	Cubic ($Fd\bar{3}m$)	443	443	523	518	0.041	0.4
C_7B	Cubic ($P\bar{4}3m$)	388	388	376	330	0.699	7.0
C_3B	Rhombohedral	333	333	269	238	0.650	6.5
C_5B_3	Orthorhombic	322	295	258	213	1.160	11.6

We find from Tables 5 that all the elastic constants obtained for the different materials satisfy the condition given by inequality (Equation 12).

The cubic system only has 3 independent elastic constants and as a sufficient condition for mechanical stability, these constants have to satisfy the inequalities:

$$C_{11} - C_{12} > 0\,;\; C_{11} + 2C_{12} > 0. \tag{13}$$

The inequalities (Equation 13) are satisfied by the diamond and C_7B results in Tables 5, it follows that these two cubic structures are mechanically stable.

The rhombohedral class has 6 independent elastic constants. Sufficient Born conditions for this class as modified by Mouhat and Coudert (2014), are given by the inequalities:

$$\left.\begin{aligned} &C_{11} > |C_{12}|; \\ &C_{13}^2 < \tfrac{1}{2}C_{33}(C_{11} + C_{12}); \\ &C_{14}^2 < \frac{1}{2}C_{44}(C_{11} - C_{12}). \end{aligned}\right\} \tag{14}$$

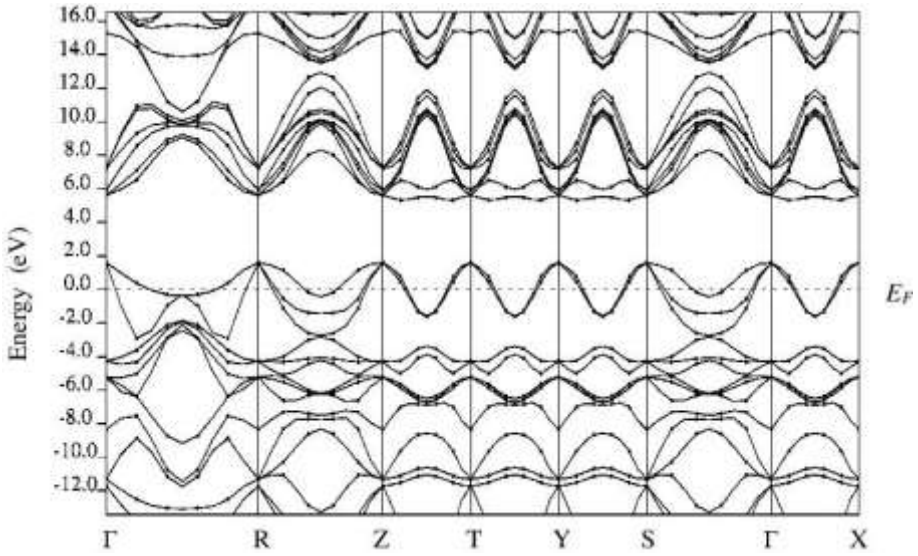

Figure 4. The Band Structure for *c*-C_7B at 0 GPa. The origin of the energy axis lies at the Fermi level, E_F.

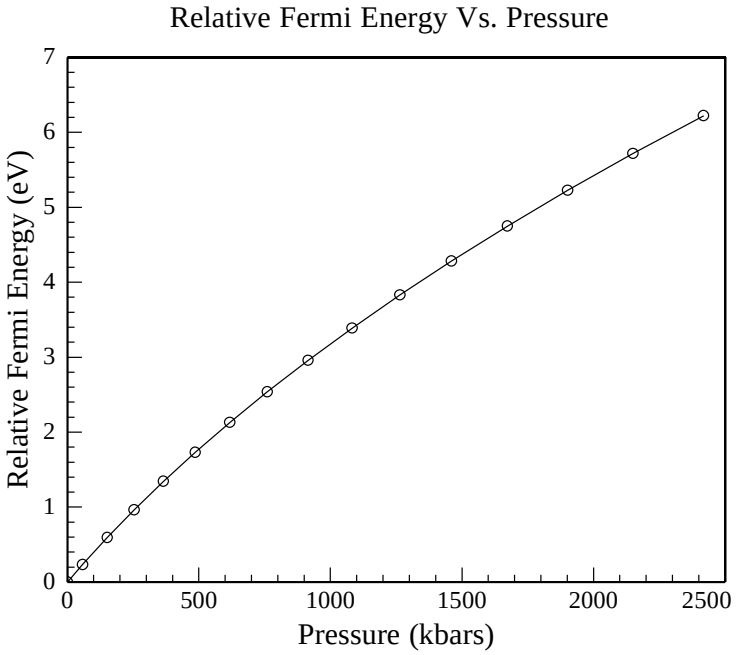

Figure 5. A graph of the Fermi energy, relative to the Fermi energy at p = 0 kbars $\left(E_F - E_F^{(0)}\right)$, plotted against the applied pressure, for *c*-C_7B.

The inequalities (Equation 14) are satisfied by the C_3B (or C_6B_2) results in Tables 5, it follows that this rhombohedral structure is mechanically stable.

The orthorhombic system has 9 independent elastic constants. A sufficient Born condition for this system (Born and Huang, 1954) is given by the inequality:

$$C_{11}C_{22}C_{33} + 2C_{12}C_{13}C_{23} - C_{11}C_{23}^2 - C_{22}C_{13}^2 - C_{33}C_{12}^2 > 0. \quad 15)$$

The inequality (Equation 15) is satisfied by the C_5B_3 results in Table 5, it follows that *o*-C_5B_3 is mechanically stable.

Figure 6 is a graph of the values of the Young, shear

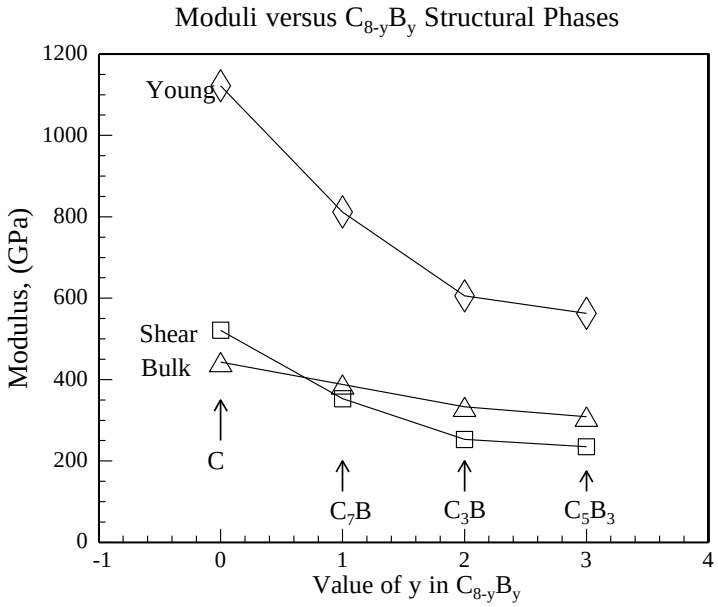

Figure 6. Graph for the trend in bulk, shear and Young moduli in $C_{8-y}B_y$ materials.

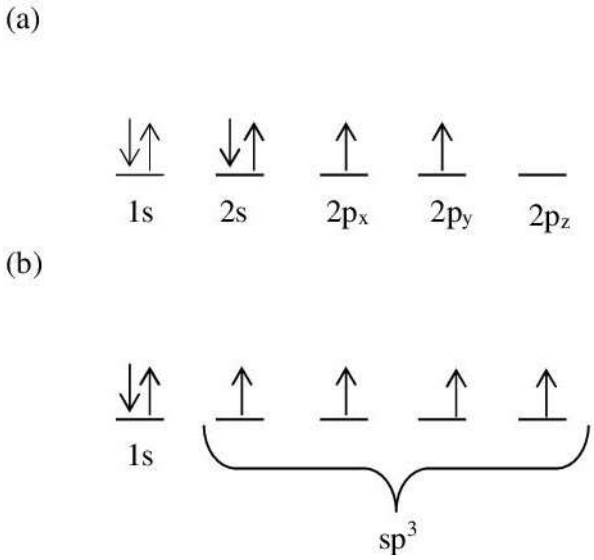

Figure 7. (a) Valence electronic pairing of 1s and 2s spins, while 2p electron spins are not paired. (b) Hybridization resulting in sp^3 hybrid orbitals having equals energies.

bulk moduli plotted against the values of *y* in $C_{8-y}B_y$ materials. The three moduli are seen to reduce in magnitude as the boron content increases.

The brittleness of a material is reflected by the ratio *B*/*G*. As reported by Pugh (1954), the critical value of this ration is *B*/*G*=1.75, for ductile materials *B*/*G*>1.75. The ratio is less than 1.75 for brittle materials. As seen in Table 6, the four materials under study are all brittle with diamond being the most brittle. C_3B and C_5B_3 are the least brittle with a *B*/*G* value of 1.32.

The Young modulus relates a stress to the resultant strain in the direction of the stress. The lateral and axial strains are related by the Poison ratio, which gives an indication of the stability of a material in relation to resistant shear and also the magnitude of the change in volume of a crystal during uniaxial deformation. The

plasticity of a material increases with an increase in the Poisson ratio. The results in Table 6 indicate that the plasticity of the materials generally increases with increased boron content.

Table 7 shows that diamond has the lowest degree of anisotropy with a Universal Elastic Anisotropy Index of only 0.041. C_5B_3 has the highest anisotropy (A_U = 1.160), this material is therefore likely to be the most susceptible to micro-cracks. The table shows that $B_V = B_R$ for the two cubic structures, C and C_7B as expected. Interestingly, the same condition is observed for C_3B which is not cubic, indicating that this material is also isotropic in terms of the bulk modulus alone.

There are a combination of mechanisms responsible for the observed reduction in magnitude of the three moduli of elasticity as the boron content increases. These same mechanisms are responsible for the general increase in plasticity and decrease in brittleness with increased boron content. The underlying mechanism is the sp^3 hybridization in the orbitals of the carbon atoms.

The creation of hybrid orbitals in carbon atoms during material synthesis is illustrated in Figure 7. Figure 7a shows the pairing of 1s and 2s spins, while 2p electron spins are not paired and are available for covalent bonding. A 2s electron can be excited, during material synthesis, to the p level resulting in four similar hybridized (mixed) sp^3 orbitals as shown in Figure 7b. It is these orbitals that form the strongest covalent bonds in nature; they are highly resistant to plastic and elastic deformations. In general, the more the hybrid C-C bonds you have in a boron/carbon material, as opposed to C-B bonds, the higher the magnitude of the three moduli of elasticity (Sun et al., 2001; Nozaki and Itoh, 1996). However, there are other factors that may come into play. The shorter the bonds and the denser they are the higher the magnitude of the three moduli, the crystal structure of the materials affects the length and density of the bonds. A combination of these factors affects the plasticity and brittleness of the materials with increased boron content. Factors like the iconicity of the bonds also play a part. Some theoretical models have been developed to relate these fundamental factors to the hardness of materials (Bao et al., 2018, 2020).

Conclusion

Low Gibbs free energy polymorphs of diamond-like materials of the type C_{8-y} B_y where y = 0 to 7, were identified at absolute zero of temperature. It has been determined that the four materials: diamond (C), cubic C_7B (c-C_7B), rhombohedral C_3B (r-C_3B) and orthorhombic C_5B_3 (o-C_5B_3) are all both dynamically and mechanically stable. The bulk modulus results in Table 6 indicate that these compounds are potentially super-hard; the values of their bulk moduli being greater than 250 GPa (Lowther, 2000). Figure 6 suggests that the hardness reduces with increasing boron content. As seen in Table 6, the materials under study are all brittle with diamond being the most brittle. C_3B and C_5B_3 are the least brittle with B/G values of 1.32. Table 7 shows that diamond has the lowest degree of anisotropy with a Universal Elastic Anisotropy Index of only 0.041 while C_5B_3 has the highest anisotropy (A_U = 1.160), which makes the latter material most susceptible to micro-cracks. Our electronic band structure calculations for cubic C_7B, which was predicted to be the hardest in the C_{8-y} B_y system after diamond, indicate that the highest valence energy band of the material crosses over the Fermi level up to about 1.7 eV above it. On the other hand, there is a band gap between the top of the valence band and the bottom of the conduction band. The material, c-BC_7 is therefore a hole-type conductor, similar to heavily boron doped diamond (Lee and Pickett, 2004). This is understandable because boron is an acceptor with one less electron in the B_xC_y valence matrix, hence functioning as a hole-dopant.

When carrying out a cost-benefit ratio analysis for the industrialization of the materials studied in this article, it should be noted that our results and the available literature indicates that the synthesis of materials with hardness exceeding that of diamond is highly unlikely, if not impossible (Solozhenko and Godec, 2019). The economical approach should therefore be to synthesize or design materials for niche applications, materials that are harder than cubic boron nitride and more useful than diamond in terms of thermal and chemical stability. Such novel materials have great prospects for the creation of new technologies required for emerging applications and their world market is inexhaustible (Solozhenko and Godec, 2019). It is hopeful that the materials studied during this project, particularly cubic C_7B, will qualify for viable niche industrial applications, through experimental evaluation.

CONFLICT OF INTERESTS

The authors have not declared any conflict of interests.

ACKNOWLEDGEMENT

The authors thank Institutional facilities of both the Copperbelt and Mukuba Universities used during the course of this research work.

REFERENCES

Bao L, Qu D, Kong Z, Duan Y (2020). Predictions of structural, electronic, mechanical, and thermodynamic properties of TMBCs (TM= Ti, Zr, and Hf) ceramics. Journal of the American Ceramic Society 103(9):5232-5247.

Bao W, Liu D, Daun Y (2018). A first-principles prediction of anisotropic elasticity and thermal properties of potential superhard WB3. Ceramics International 44(12):14053-14062.

Baroni S, Giannozzi P, Testa A (1987). Green's-function approach to linear response in solids. Physical review letters 58(18):1861.
Born M, Huang K (1954). Dynamics Theory of Crystal Lattices, Oxford University Press.
Clerc DG (1999). Ab initio elastic properties of diamond-like materials: electronic factors that determine a high bulk modulus. Journal of Physics and Chemistry of Solids 60(1):103-110.
Gao Y, Wu Y, Huang Q, Ma M, Pan Y, Xiong M, Li Z, Zhao Z, He J, Yu D (2018). First principles studies of superhard BC6N phases with unexpected 1D metallicity. Computational Materials Science 148:157-164.
Ghosh A, Gusmão MS, Chaudhuri P, de Souza SM, Mota C, Trichês DM, Frota HO (2016). Electrical properties of SnSe under high-pressure. Computational Condensed Matter 9:77-81.
Giannozzi P, Baroni S, Bonini N, Calandra M, Car R, Cavazzoni C, Ceresoli D, Chiarotti GI, Cococcioni M, Dabo I, Dal Corso A, de Gironcoli S, Fabris S, Fratesi G, Gebauer R, Gerstmann U, Gougoussis C, Kokalj A, Lazzeri M, Martin-Samos I, Marzari N, Mauri F, Mazzarello R, Paolini S, Pasquarello A, Paulatto I, Sbraccia C, Scandolo S, Sclauzero G, Seitsonen AP, Smogunov A, Umari P, Wentzcovitch RM (2009). QUANTUM ESPRESSO: a modular and open-source software project for quantum simulations of materials. IOP Publishing Ltd. Journal of Physics: Condensed Matter 21(39):395502. https://doi.org/10.1088/0953-8984/21/39/395502
Giannozzi P, de Gironcoli S, Pavone P, Baroni S (1991). Ab initio calculation of phonon dispersions in semiconductors. Physical Review B 43(9):7231.
Golesorkhtabar R, Pavone P, Spitaler J, Puschnig P, Draxl C (2013). ElaStic: A tool for calculating second-order elastic constants from first principles. Computer Physics Communications 184(8): 1861-1873.
Habanyama A, Msikita M, Simfukwe J, Baliga GT, Mumba NK, Mulenga M Samukonga G (2018). Study of ultra-hard materials of the BCNO quaternary system. Results in Physics 11:984-993.
He XL, Shao X, Chen T, Tai YK, Weng XJ, Chen Q, Dong X, Gao G, Sun J, Zhou XF, Tian Y, Wang HT (2019). Predicting three-dimensional icosahedron-based boron B60. Physical Review B 99(18): 184111. https://doi.org/10.1103/PhysRevB.99.184111
Hill R (1963). Elastic properties of reinforced solids: some theoretical principles. Journal of the Mechanics and Physics of Solids 11(5):357-372.
Hu YJ, Xu SL, Wang H, Liu H, Xu XC, Cai YX (2016). Superhard BC2N: an Orthogonal Crystal Obtained by Transversely Compressing (3, 0)-CNTs and (3, 0)-BNNTs. Chinese Physics Letters, 33(10):106102.
John P, Polwart N, Troupe CE, Wilson JIB (2002). The oxidation of (100) textured diamond. Diamond and related materials 11(3-6):861-866.
Kohn W, Sham L (1965). Self-consistent equations including exchange and correlation effects. Physical review 140(4A):A1133.
Kokalj A (2003). Computer graphics and graphical user interfaces as tools in simulations of matter at the atomic scale. Computational Materials Science 28(2):155-168.
Kvashnin AG, Allahyari Z, Oganov AR (2019). Computational discovery of hard and superhard materials. Journal of Applied Physics 126(4):040901.
Ledbetter H, Migliori A (2006). A general elastic-anisotropy measure. Journal of applied physics 100(6):063516.
Lee KW, Pickett WE (2004). Superconductivity in boron-doped diamond. Physical review letters, 93(23):237003.
Lowther JE (2000). Superhard materials. Physica status solidi (b). 217(1):533-543.
Mazhnik E, Oganov AR (2019). A model of hardness and fracture toughness of solids. Journal of Applied Physics 126(12):125109.
Monkhorst HJ, Pack JD (1976). Special points for Brillouin-zone integrations. Physical review B, 13(12):5188.
Mouhat F, Coudert FX (2014). Necessary and sufficient elastic stability conditions in various crystal systems. Physical review B 90(22):224104.
Nassau K, Nassau J (1979). The history and present status of synthetic diamond. Journal of Crystal Growth 46(2):157-172.
Niu H, Niu S, Oganov AR (2019). Journal of Applied Physics 125(6):065105.
Nozaki H, Itoh S (1996). Structural stability of BC2N. Journal of Physics and Chemistry of Solids 57(1):41-49.
Perdew JP, Burke K, Ernezerhof M (1996). Generalized Gradient Approximation Made Simple. Physical Review Letters. 77:3865.
Ranganathan SI, Ostoja-Starzewski M (2008). Universal elastic anisotropy index. Physical Review Letters 101(5):055504.
Reuss A, Angew Z (1929). Berchung der Fließgrenze von Mischkristallen auf Grund der Plastizitätsbedingung für Einkristalle. Journal of Applied Mathematics and Mechanics (Zeitschrift für Angewandte Mathematik und Mechanik) 9(1):49-58. https://doi.org/10.1002/zamm.19290090104
Singh BP (1986). Characterization of cubic boron nitride compacts. Materials research bulletin. 21(1):85-92.
Solozhenko VL, Godec YL (2019). A hunt for ultrahard materials. Journal of Applied Physics 126:230401 https://doi.org/10.1063/1.5139489
Solozhenko VL, Gregoryanz E (2005). Synthesis of superhard materials. Materials Today 8(11):44-51.
Stavrou E, Lobanov S, Dong H, Oganov AR, Prakapenka VB, Konˆopkov´a Z Goncharov AF (2016). Synthesis of ultra-incompressible sp3-hybridized carbon nitride with 1: 1 stoichiometry. Chemistry of Materials 28(19):6925-6933.
Sun H, Jhi SH, Roundy D, Cohen ML, Louie SG (2001). Structural forms of cubic BC 2 N. Physical Review B. 64(9):094108.
Voigt W (1928). Lehrbuch der Kristallphysik, (Textbook of crystal physics). BG Teubner, Leipzig und Berlin.
Yanchitsky BZ, Timoshevskii AN (2001). Determination of the space group and unit cell for a periodic solid. Computer physics communications 139(2):235-242.
Zhao Z, Xu B, Tian Y (2016). Recent advances in superhard materials. Annual Review of Materials Research 46:383-406.